

Alloying Behaviour and Microstructural Changes of a Ti-10%Mo-10%Cr Alloy on Sintering Process

(Sifat Pengaloiian dan Perubahan Mikrostruktur Aloji Ti-10%Mo-10%Cr ke atas Proses Sinter)

JUNAIDI SYARIF*, EKO KURNIAWAN, TUBAGUS N. ROHMANNUDIN, MOHAMAD RASIDI RASANI & ZAINUDDIN SAJURI

ABSTRACT

This study aimed to investigate the effects of element diffusion on the alloying behaviour and microstructure of a Ti-10%Mo-10%Cr alloy during sintering and furnace cooling. A theoretical calculation of the average diffusion distance for each element was performed to predict the alloying behaviour during sintering and furnace cooling. The Ti-10%Mo-10%Cr alloy was fabricated using a blended element powder metallurgy approach. Micrograph of the samples after sintering showed bright-circle structures and significantly decreased equiaxed structures. The number of plate-like structures increased with prolonged sintering time. Microstructural changes occurred because of element diffusion resulting from the prolonged sintering time. Moreover, the diffusion distance of each element also increased with prolonged sintering time. Although elements can sufficiently diffuse during both sintering and furnace cooling, the diffusion distance during sintering was considerably higher than that during furnace cooling for all elements. The diffusion distances of Cr and Mo were the highest and lowest, respectively, during sintering and furnace cooling. This study showed that alloying behaviour mostly occurred during sintering and was controlled by the diffusion of Mo atoms.

Keywords: Diffusion; microstructure; powder metallurgy; sintering; Ti alloy

ABSTRAK

Kajian ini bertujuan untuk mengkaji kesan peresapan unsur terhadap kelakuan pengaloiian dan mikrostruktur pada aloji Ti-10%Mo-10%Cr semasa sinteran dan penyejukan relau. Pengiraan secara teori terhadap jarak peresapan purata bagi setiap unsur dilakukan untuk meramal kelakuan pengaloiian semasa sinteran dan penyejukan relau. Aloji Ti-10%Mo-10%Cr telah direka menggunakan pendekatan metalurgi serbuk unsur sehati. Mikrograf sampel selepas pensinteran menunjukkan struktur bulatan-terang dan struktur sama paksi yang menurun secara ketara. Bilangan struktur seperti plat meningkat dengan memanjangkan masa pensinteran. Perubahan mikrostruktur berlaku disebabkan penyebaran unsur yang dihasilkan semasa pensinteran yang berpanjangan. Selain itu, jarak resapan bagi setiap elemen juga meningkat dengan masa pensinteran berpanjangan. Walaupun unsur-unsur boleh cukup meresap semasa sinteran dan penyejukan relau, jarak resapan semasa sinteran adalah lebih tinggi daripada semasa penyejukan relau untuk semua unsur. Jarak peresapan Cr dan Mo masing-masing yang tertinggi dan terendah, semasa sinteran dan penyejukan relau. Kajian ini menunjukkan bahawa kelakuan pengaloiian kebanyakannya berlaku semasa sinteran dan dikawal oleh resapan atom Mo.

Kata kunci: Aloji Ti; metalurgi serbuk; mikrostruktur; pensinteran; peresapan

INTRODUCTION

In recent years, BCC (β) type Ti alloys have received considerable attention for biomaterial applications because of their specific strength, excellent corrosion resistance, biocompatibility and low elastic modulus of the β -Ti alloys (Leyens & Peters 2003). Niinomi (2003) also showed that Ti alloys have excellent biocompatibility, especially for dental applications. Moreover, Oliveira and Guastaldi (2009) reported that Ti alloys are promising biomaterials because they have good corrosion resistance. Since the biocompatibility of alloys is important, therefore the safest alloying elements (Nb, Ta, Zr, Mo and Sn) for the human body must be selected for the development new β -type titanium alloys (Niinomi 2003, 2002). However,

the biomaterial applications of titanium are limited by the high cost of this element (Carman et al. 2011). Moreover, Niinomi (2003) stated that materials for dental application that are often fabricated through casting are difficult to be treated because of inaccurate high-precision products.

On the other hand, inexpensive powder metallurgy (PM) techniques can also be used to fabricate Ti alloys (Carman et al. 2011). Fujita et al. (1996) demonstrated that the Ti-4.5Al-3V-2Fe-2Mo alloy that is fabricated by a blended element powder metallurgy (BEPM) exhibits superior properties over Ti-6Al-4V alloy such as high sinterability, fine microstructure, excellent mechanical properties and good cold workability. Then, Yang et al. (2011) noted that the densification of sintered product can be achieved by the BEPM process. In BEPM, powder

elements are blended with a master element, cold pressed and then sintered to a higher density (Hagiwara & Emura 2003). Moreover, the PM technique can fabricate parts with near net-shapes at a large scale and with relatively low cost (Abkowitz et al. 2015).

In our previous work, authors developed a new β -Ti alloy by BEPM and showed that the alloy exhibits a single β -phase after sintering and solution treatment with quenching (Syarif et al. 2013, 2008). However, the diffusion behavior of the alloying element during sintering and furnace cooling remains unclear. In this study, the effect of element diffusion on the alloying behavior and microstructural change was investigated on a Ti-10%Mo-10%Cr alloy that is subjected to sintering and furnace cooling.

MATERIALS AND METHODS

A Ti-10%Mo-10%Cr alloy was used as the specimen in this study. In our previous work, the alloy showed a single β phase after sintering at 1573 K for 14.4 ks and solution treatment at 1573 K for 1.8 ks (Syarif et al. 2013). Commercially pure Ti, Mo, and Cr powders were used as raw materials. All of the powders were supplied by Alfa Aesar (USA). Table 1 shows the purities and particle sizes of the powders used.

Ti powder as the master element was mechanically blended with 10%Mo and 10%Cr as the alloying element powders for 3.6 ks. The blended powder was loaded into a die cavity with a diameter of 10 mm and compressed by

TABLE 1. Particle size and purity of powders used

Element	Particle size/ mesh	Purity /%
Ti	-325	99.0
Mo	-170	99.5
Cr	-325	99.0

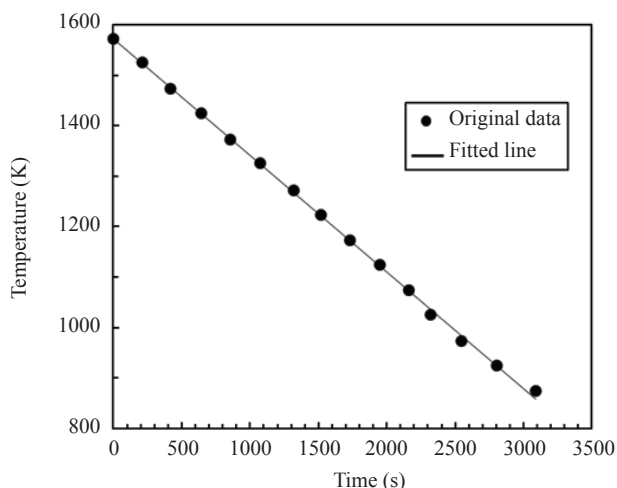


FIGURE 1. Relation between temperature and time on furnace cooling from 1573 K to 873 K from experiment result in vacuum furnace. The fitted line is linear regression for calculating cooling rate (λ)

cold compaction under a pressure of 1000 MPa for 3.6 ks at ambient temperature. The sample was sintered at 1573 K for 0.6 ks to 14.4 ks and then furnace-cooled under an argon gas atmosphere after achieving vacuum conditions. In the furnace, the cooling rate (λ) was approximately 0.23 K/s when cooled from 1573 K to 873 K (Figure 1).

The microstructure of the alloy was observed by optical microscope and scanning electron microscope (SEM). Samples for microstructural observation were etched using Kroll's reagent. The distribution of elements in the sample was analyzed using SEM–energy dispersive X-ray spectroscopy (EDS). Phase characterization was performed using X-ray diffractometry (XRD) with Cu-K α radiation. The phase evolution during furnace cooling was predicted using commercial software (JMatPro™).

RESULTS AND DISCUSSION

MICROSTRUCTURAL CHANGES IN THE TI-10%MO-10%CR ALLOY

Figure 2 shows the microstructure of the Ti-10%Mo-10%Cr alloy. In the 1.8 ks-sintered sample, bright-circle structures, equiaxed structures and pores were observed. Equiaxed structures were shown in the vicinity of the bright-circle structures, whereas needle-like structures were located far from the bright-circle structures. The needle-like structures indicate the presence of a dual-phase structure in the 14.4 ks-sintered sample. The formation of the needle-like structures was due to sympathetic nucleation, as reported by Lütjering and Williams (2007), the hcp (α) phase will nucleate and grow within β grains and along β grain boundaries and $\alpha + \beta$ lamella will be formed during furnace cooling from the β phase region. The volume fraction of all structures changed as the sintering time was increased. As shown in Figure 3, the volume fraction of each structure changed as a function of the sintering time. The amount of bright-circle and equiaxed structures decreased as the sintering time increased. The volume fraction of the pores slightly increased, although interparticle bonding occurred during sintering. Shewmon (1989) stated that the pores were formed because of the Kirkendall effect. The amount of the bright-circle and equiaxed structures decreased because of the formation of needle-like structures during sintering. The alloying behavior and the interparticle bonding of the blended pure metallic powders were enhanced by diffusion of elements during sintering.

To further analyze the alloying behavior, the samples were subjected to XRD. The XRD diffractograms of the samples are shown in Figure 4. The XRD diffractogram of the green compact is also shown. In this figure, the peaks of the pure Mo and Cr powders disappeared after 0.6 ks of sintering and β phase peaks can be observed alongside the peaks corresponding to the α phase in the alloy. The peak intensity of the α phase increased as the sintering time was increased. This result indicates that the increase in the volume fraction of needle-like structures can be

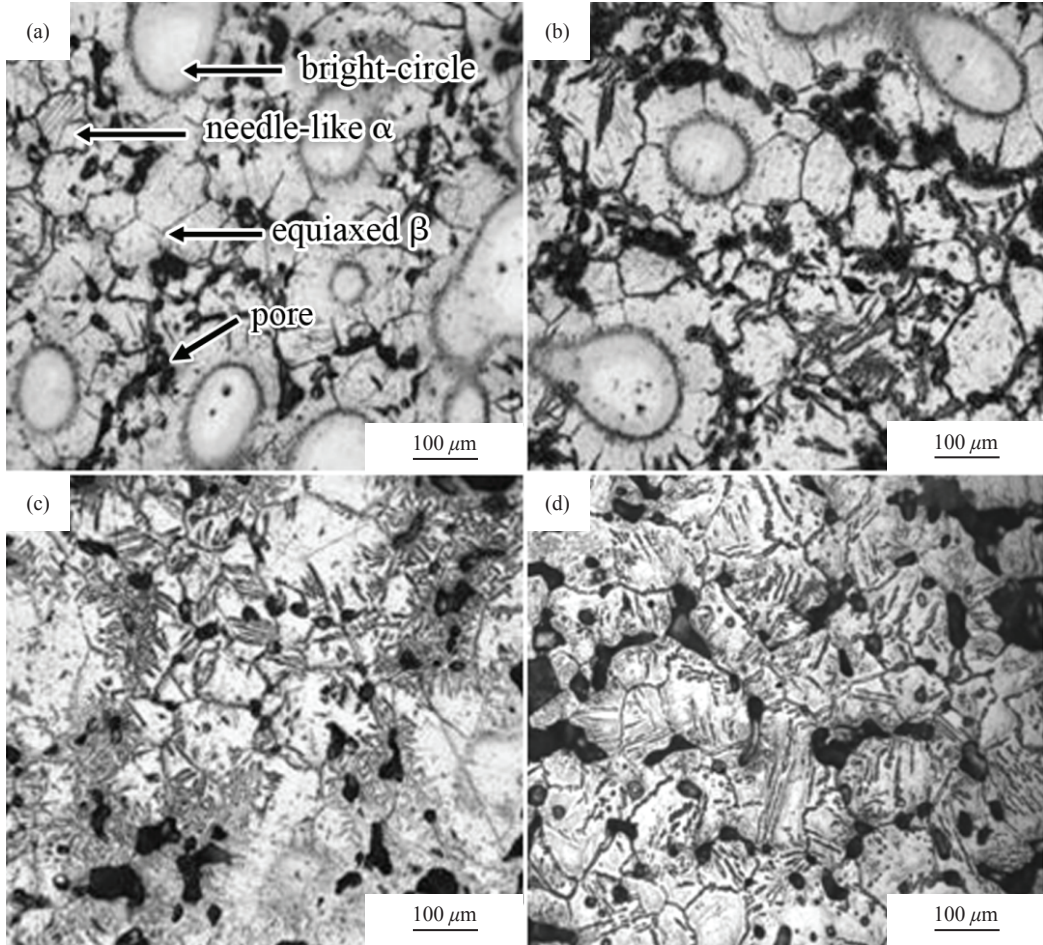


FIGURE 2. Micrograph of the samples after sintering at (a) 0.6 ks; (b) 1.8 ks; (c) 5.4 ks; and (d) 14.4 ks and followed by furnace cooling

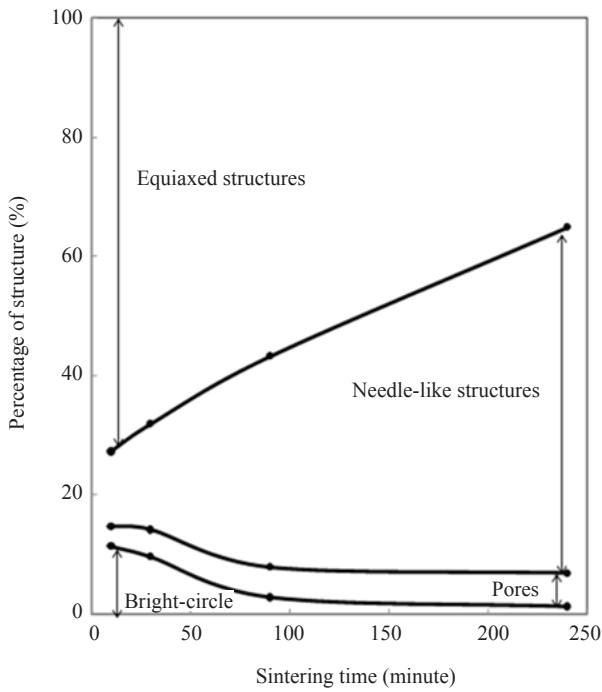


FIGURE 3. Schematic diagram of alloying behavior during sintering process and followed by furnace cooling

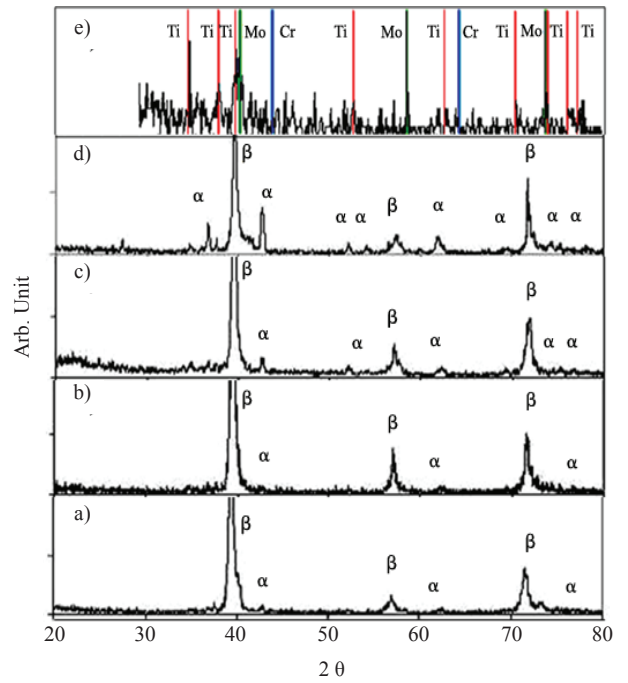


FIGURE 4. XRD diffractograms of the (a) 0.6 ks; (b) 1.8 ks; (c) 5.4 ks; and (d) 14.4 ks sintered sample and (e) green sample

attributed to the formation of needle α structures in the sintered sample. Thus, the XRD results are consistent with the result depicted in Figure 3. Alloying of the blended pure powders occurred during sintering and furnace cooling, although the single β phase was not obtained through this process.

ALLOYING BEHAVIOR

The atomic distribution and chemical concentration of all elements were examined by SEM-EDS to clarify the contribution of element diffusion to the alloying behavior. Figure 5 presents backscattered electron (BSE) images and mapping of element distribution of the sample sintered at 1573 K for 0.6 ks. Two microstructures were observed from the sample: The first was a bright-circle structure within a dark region (Figure 5(a)) and the other was a needle-

like structure (Figure 5(b)). The bright-circle structure within the dark region was identical to the bright-circle and equiaxed microstructures shown in Figure 2(a). In the bright-circle structures, Cr atoms were uniformly distributed within the sample. Conversely, the distribution of Mo and Ti atoms exhibited the opposite distribution. Ti atoms were dispersed uniformly in the dark region, whereas Mo atoms were concentrated almost entirely in the bright-circle structures. The pure Mo powder was still not dissolved during this process. As shown in Figure 5(b), all atoms of the alloying elements were uniformly distributed within the needle-like structures.

Figure 6 shows the BSE images and mapping of element distribution of the 5.4 ks-sintered sample. The element distributions were also analyzed in the bright-circle and needle-like structures for the 5.4 ks-sintered sample. In the bright-circle structures, Mo atoms were

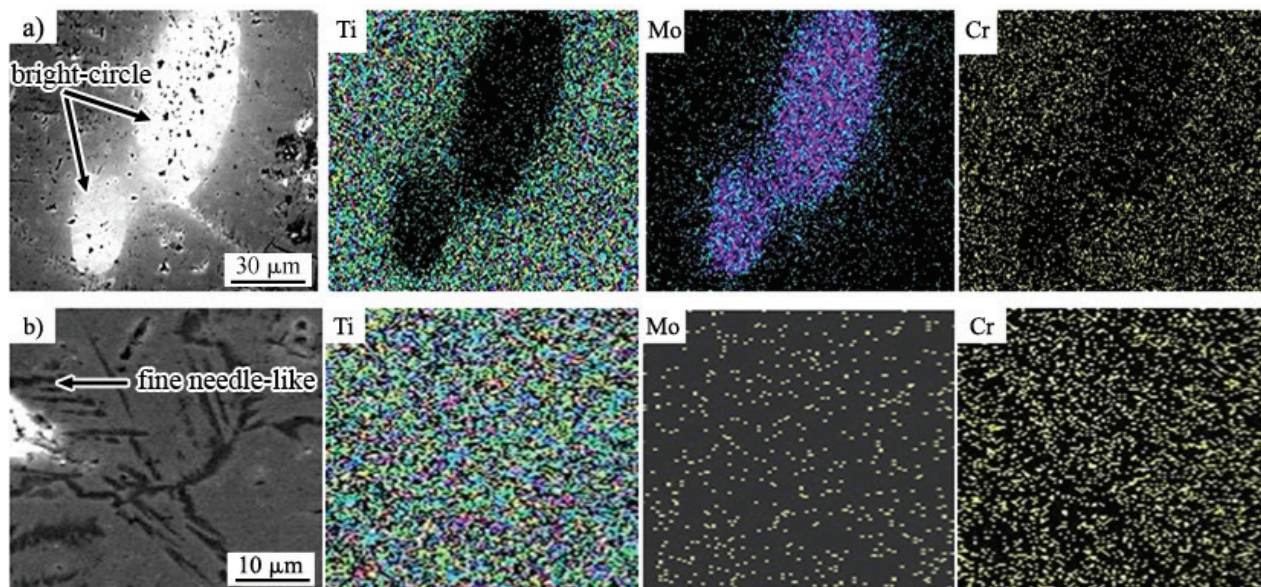


FIGURE 5. Mapping of element distribution in (a) bright circle structure and (b) fine needle-like structure for 0.6 ks sintered sample

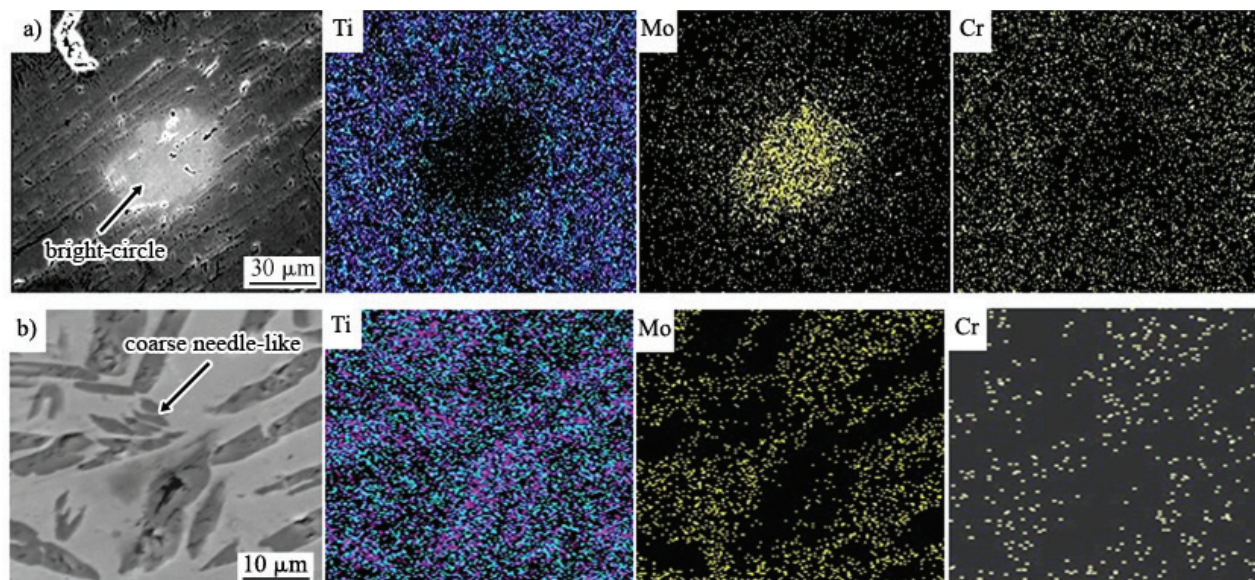


FIGURE 6. Mapping of element distribution in (a) bright circle structure and (b) coarse needle-like structure for 5.4 ks sintered sample

still enriched in the bright-circle while Ti atoms were distributed in the dark region, although Cr atoms were well dispersed in the entire region. As shown in Figure 6(a), Ti atoms were completely distributed in all whitish and darkish areas. Conversely, Mo and Cr atoms were slightly enriched in the whitish area. Thus, the whitish area was believed to represent the β phase because Mo and Cr atoms are the β phase former.

Table 2 shows the average concentrations of the elements in all of the microstructures for the 0.6 ks- and the 5.4 ks-sintered samples. The average concentration was measured by SEM-EDS to quantitatively analyze the element composition of the microstructures shown in Figures 5 and 6. The average concentrations of Cr were almost identical to the designated Cr concentration of 10% in all microstructures. However, a significant difference in the Mo concentration was observed between the 0.6 ks and 5.4 ks-sintered samples.

The bright-circle structures in both the 0.6 ks- and 5.4 ks-sintered samples had higher Mo concentrations than the designated Mo concentration (10%), although the Mo concentration decreased as the sintering time was increased. In contrast to the previous result, the average concentration of Mo in the needle-like structures increased as the sintering time was prolonged and almost reached the designated concentration. These results suggested that the alloying behavior has occurred during sintering and furnace cooling and that the diffusion of Mo atoms controlled the alloying behavior.

TABLE 2. Average concentrations of elements in microstructures of the 0.6ks- and the 5.4ks-sintered samples

Sintering time	Microstructure	Concentration of element (%)		
		Ti	Mo	Cr
0.6ks	Bright-circle structure	74.1	16.7	8.1
0.6ks	Fine needle-like structure	84.9	4.3	9.8
5.4ks	Bright-circle structure	75.7	14.7	9.6
5.4ks	Coarse needle-like structure	77.3	11.5	11.2

DIFFUSION OF ALLOYING ELEMENTS

The diffusion of elements and the formation of needle-like structures were enhanced in the process, although the sample was sintered for a short time (0.6 ks). Thus, element diffusion occurred not only during sintering at high temperatures but also during furnace cooling, because the cooling rate was sufficiently low.

The diffusion of element during sintering is usually expressed as follows (Kakani 2004).

$$D_{el} = D_0 \exp[-Q/(RT)] \quad (1)$$

where D_{el} is the diffusion coefficient of each element; D_0 is the temperature-independent pre-exponential factor; Q is the activation energy; R is the gas constant (8.31 J/mol.K); and T is the sintering temperature (1573 K). Table 3 summarizes the D_0 and Q values for Ti, Mo and

Cr (Shackelford & Alexander 2010). The phase prediction using JmatProTM indicated that the sample was in the β phase region during sintering at 1573 K. Thus, the element diffusion was calculated based on the diffusion parameters in the β matrix, yielding diffusion coefficients of 16.36×10^{-13} , 8.35×10^{-13} and 65.53×10^{-13} m²/s for Ti, Mo, and Cr, respectively. Consistent with the results of Nakajima and Koiwa (1991) the diffusion coefficient of Mo was the lowest compared to those of Ti and Cr. This result can be attributed to the larger atomic size of Mo, which results in lower activation energy compared with Ti and Cr (Table 3).

TABLE 3. Diffusion data of elements

Element	Prefactor D_0 (m ² .s ⁻¹)	Activation energy Q (J.mol ⁻¹)	Temperature T (K)
α -Ti	8.6×10^{-10}	150306.12	973 - 1123
β -Ti	3.58×10^{-8}	130628.16	1173 - 1813
Cr	5×10^{-7}	146956.68	1223 - 1873
Mo	8×10^{-7}	180032.40	1173 - 1873

Shackelford & Alexander 2010

Then, the average diffusion distance of each element can be estimated using Einstein's equation (Atkins & De Paula 2006; Philibert 1991) as follows.

$$\bar{x}_s = \sqrt{2D_{el}t_s} \quad (2)$$

where \bar{x}_s is the linear distance travelled by diffusivity in one dimension; and t_s is the sintering time. The sintering times varied from 0.6 to 14.4 ks. Figure 7 shows the relation between the average diffusion distance and the sintering time t_s . In general, the diffusion distance of all elements increased as the sintering time was increased.

On the other hand, the average diffusion distance of each element during furnace cooling was also calculated. Our simulation using JmatProTM predicted that the β phase decomposes into an $\alpha+\beta$ phase at temperatures of 773 K or below during furnace cooling. It is predicted that the diffusion of element will be very slow in the α phase and at temperature of 773 K; thus, the average diffusion distance calculation was conducted in the range of 1573 K to 873 K and in the β matrix.

Balluffi et al. (2005) defined the temperature during furnace cooling as follows,

$$T = \frac{T_0}{1 + \frac{t}{\lambda}} \quad (3)$$

where T_0 and λ are the initial temperature and cooling rate, respectively.

Furthermore, Shewmon (1989) explained that diffusion during cooling is a function of cooling time. The average diffusion distance during cooling can be expressed as

$$\Theta = \int_0^{t_c} D(t) \partial t \quad (4)$$

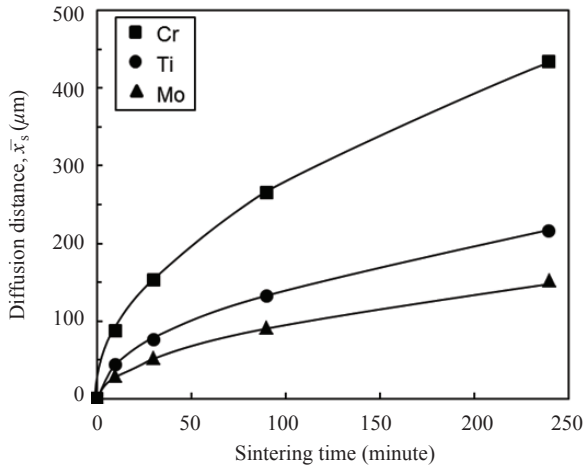


FIGURE 7. The average diffusion distance of each element as a function of sintering time

where Θ is the average diffusion distance during cooling and $\partial\Theta = D(t)\partial t$. The unit of Θ is μm^2 .

According to Ganguly (2002) and (2008), the diffusion during cooling is strongly dependent on the cooling time; hence, the diffusion coefficient can be modified by substituting (3) into (1),

$$D(t) = D_0 e^{-\frac{Q(1+\frac{t}{\lambda})}{RT_0}} \quad (5)$$

Equation (5) can be simplified as follows:

$$D(t) = \Gamma e^{-t/\sigma} \quad (6)$$

where $\Gamma = D_0 e^{-Q/(RT_0)}$ and $\sigma = \lambda \left(\frac{RT_0}{Q} \right)$. The average diffusion distance can then be modified by substituting (6) into (4),

$$\Theta = \int_0^{t_c} \Gamma e^{-t/\sigma} \partial t \quad (7)$$

and integrating from t_c to t_c as the time during cooling (Figure 1), to give the average diffusion distance. Finally, the total diffusion distance of each element during furnace cooling can be obtained by substituting the result from (7) into (2),

$$\bar{x}_s = \sqrt{2\Theta} \quad (8)$$

The relation between the total diffusion distances of each element during cooling as a function of cooling time was calculated and is shown in Figure 8. In the figure, the top x-axis exhibits the sample's temperature after cooling for certain time, which is shown in the bottom x-axis. The temperature was calculated by (3). It is predicted that the diffusion distance increased as the cooling time was increased. The diffusion distance of Cr was the highest among the elements. Conversely, the diffusion distance of Mo was the smallest during cooling. The rates of furnace cooling were the same in all samples; thus, the comparative order of total diffusion distances during cooling between elements is $\text{Cr} > \text{Ti} > \text{Mo}$ (Table 4). However, the diffusion distance during furnace cooling was obviously one-tenth or smaller than that during sintering for all elements.

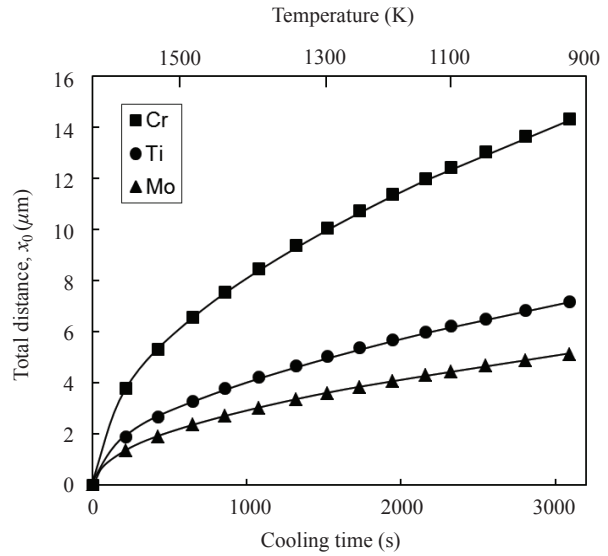


FIGURE 8. Diffusion distance of each element as a function of cooling time in β -phase with cooling rate 0.23 K/s

TABLE 4. Total diffusion distance on cooling of each element

Element	(μm)
β -Ti	7.2
Cr	14.3
Mo	5.1

Thus, alloying behavior can be observed mostly during sintering. Moreover, the alloying behavior is controlled by the diffusion of Mo atoms because Mo atoms showed the smallest diffusion distance. Therefore, this phenomenon may explain why some Mo particles were still present after sintering for 5.4 ks and furnace cooling (Figures 5 and 6). This calculation agrees well with the observed experimental result that the diffusion of Mo atoms restrains the alloying phenomenon.

CONCLUSION

Observing the diffusion of alloying elements in Ti-10%Mo-10%Cr alloy during sintering and furnace cooling led to the following conclusions. Alloying and microstructural changes occurred during both sintering and furnace cooling. However, the alloying behavior mostly occurred during sintering. The alloying behavior was controlled by the diffusion of Mo. The Mo and Cr atoms showed the lowest and highest diffusion distances, respectively, during both sintering and furnace cooling.

ACKNOWLEDGEMENTS

The authors would like to acknowledge Universiti Kebangsaan Malaysia and the Ministry of Science, Technology, and Innovation for funding this research under Grant Arus Perdana UKM-AP-NBT-14-2010 and ERGS/1/2012/TK04/UKM/02/5, respectively.

REFERENCES

- Abkowitz, S., Abkowitz, S. & Fisher, H. 2015. Titanium alloy components manufacture from blended elemental powder and the qualification process. In *Titanium Powder Metallurgy: Science, Technology and Applications*, edited by Qian, M. & Froes, F.H. Oxford: Butterworth-Heinemann.
- Atkins, P. & De Paula, J. 2006. *Atkins' Physical Chemistry*. New York: Oxford University Press.
- Balluffi, R.W., Allen, S. & Carter, W.C. 2005. *Kinetics of Materials*. New Jersey: John Wiley & Sons, Inc.
- Carman, A., Zhang, L.C., Ivasishin, O.M., Savvakina, D.G., Matviychuk, M.V. & Pereloma, E.V. 2011. Role of alloying elements in microstructure evolution and alloying elements behaviour during sintering of a near- β titanium alloy. *Materials Science and Engineering: A* 528: 1686-1693.
- Fujita, T., Ogawa, A., Ouchi, C. & Tajima, H. 1996. Microstructure and properties of titanium alloy produced in the newly developed blended elemental powder metallurgy process. *Materials Science and Engineering: A* 213: 148-153.
- Ganguly, J. 2002. Diffusion kinetics in minerals: Principles and applications to tectono-metamorphic processes. *European Mineralogical Union Notes in Mineralogy* 4(Chapter 10): 271-309.
- Hagiwara, M. & Emura, S. 2003 Blended elemental P/M synthesis and property evaluation of Ti-1100 alloy. *Materials Science and Engineering: A* 352: 85-92.
- Kakani, S.L. 2004. *Material Science*. New Delhi: New Age International (P) Limited.
- Leyens, C. & Peters, M. 2003. *Titanium and Titanium Alloys*. Weinheim: WILEY-VCH Verlag GmbH & Co. KGaA.
- Lütjering, G. & Williams, J.C. 2007. *Titanium*. 2nd ed. Berlin: Springer-Verlag.
- Nakajima, H. & Koiwa, M. 1991. Diffusion in titanium. *ISIJ International* 31: 757-766.
- Niinomi, M. 2003. Recent research and development in titanium alloys for biomedical applications and healthcare goods. *Science and Technology of Advanced Materials* 4: 445-454.
- Niinomi, M. 2002. Recent metallic materials for biomedical applications. *Metallurgical and Materials Transactions A* 33: 477-486.
- Oliveira, N. & Guastaldi, A. 2009. Electrochemical stability and corrosion resistance of Ti-Mo alloys for biomedical applications. *Acta Biomaterialia* 5: 399-405.
- Philibert, J. 1991. *Atom Movements: Diffusion and Mass Transport in Solids*. Les Ulis: Editions de Physique.
- Shackelford, J.F. & Alexander, W. 2010. *CRC Materials Science and Engineering Handbook*. 3rd ed. Florida: Taylor & Francis.
- Shewmon, P.G. 1989. *Diffusion in Solids*. 2nd ed. New York: McGraw-Hill.
- Syarif, J., Rohmannudin, T.N., Omar, M.Z., Sajuri, Z. & Harjanto, S. 2013. Stability of the beta phase in Ti-Mo-Cr alloy fabricated by powder metallurgy. *Journal of Mining and Metallurgy, Section B: Metallurgy* 49: 285-292.
- Syarif, J., Rohmannudin, T.N., Omar, M.Z., Sajuri, Z. & Daud, A.R. 2008. Study on formation of β single phase of a Ti-10at% Mo-10at% Cr alloy on sintering and solution treatment, *Proceedings of the 1st WSEAS International Conference on Materials Science*. pp. 48-52.
- Yang, Y.F., Luo, S.D., Schaffer, G.B. & Qian, M. 2011. Sintering of Ti-10V-2Fe-3Al and mechanical properties. *Materials Science and Engineering: A* 528(22-23): 6719-6726.
- Zhang, Y. 2008. *Geochemical Kinetics*. New Jersey: Princeton University Press.

Junaidi Syarif
University of Sharjah
College of Engineering, Sharjah
UAE

Eko Kurniawan, Tubagus N. Rohmannudin, Mohamad Rasidi Rasani & Zainuddin Sajuri
Faculty of Engineering and Built Environment
Universiti Kebangsaan Malaysia
43600 UKM Bangi, Selangor Darul Ehsan
Malaysia

*Corresponding author; email: sjunaidi@sharjah.ac.ae

Received: 17 October 2016

Accepted: 25 October 2017

